SAE INTERNATIONAL®

Momentum Flux Measurement on Single-Hole GDI Injector under Flash-Boiling Condition

2015-24-2480

Published 09/06/2015

Lucio Postrioti, Maurizio Bosi, and Andrea Cavicchi
Università degli Studi di Perugia

Fakhry AbuZahra
Izmir Insitute of Technology

Rita Di Gioia and Giovanni Bonandrini
Magneti Marelli Powertrain SPA

CITATION: Postrioti, L., Bosi, M., Cavicchi, A., AbuZahra, F. et al., "Momentum Flux Measurement on Single-Hole GDI Injector under Flash-Boiling Condition," SAE Technical Paper 2015-24-2480, 2015, doi:10.4271/2015-24-2480.

Abstract

Direct Injection technology for Spark Ignition engines is currently undergoing a significant development process in order to achieve its complete potential in terms of fuel conversion efficiency, while preserving the ability to achieve future, stringent emission limits. In this process, improving the fuel spray analysis capabilities is of primary importance. Among the available experimental techniques, the momentum flux measurement is one of the most interesting approaches as it allows a direct measurement of the spray-air mixing potential and hence it is currently considered an interesting complement to spray imaging and Phase Doppler Anemometry. The aim of the present paper is to investigate the fuel spray evolution when it undergoes flash boiling, a peculiar flow condition occurring when the ambient pressure in which the spray evolves is below the saturation pressure of the injected fluid. These thermodynamic conditions can occur in part load operation for GDI (Gasoline Direct Injection) engines, causing the spray flow structure and hence the mixture formation process to be completely altered with respect to standard flow conditions.

To investigate the effects of flash-boiling on the spray evolution, a single-hole GDI research injector designed by Magneti Marelli was analyzed in terms of both global spray shape evolution and of spray momentum flux. A preliminary injection rate analysis was also carried out to investigate the hydraulic behavior of the research injector. The spray tests were executed inside a quiescent vessel at ambient pressure ranging from 40 to 300 kPa. To obtain the flash-boiling conditions, both the injector fixture and the test fuel (*n*-heptane) temperatures were set between 30 °C and 120 °C. For the spray momentum flux tests, distances from 5 to 40 mm from the nozzle were used. Aiming to compare the internal spray structure under low and high temperature conditions, momentum spatial distribution was also investigated over planes at different distances from the nozzle. The results of this work, obtained in well-defined conditions in terms of fuel composition and spray configuration (single jet), can assist the development of CFD numerical tools as well as contribute to a better understanding of the flash-boiling phenomenon effect to the spray formation and evolution.

Introduction

In recent years, the introduction in several Countries of regulations aimed at reducing CO_2 emissions from vehicles has significantly changed the technical scenario for the development of internal combustion engines, with peculiar consequences for the spark ignited applications. This push towards more efficient combustion systems has significantly spread the Gasoline Direct Injection (GDI) technology, due to the consistent advantages offered with respect to multi-point injection technology. The adoption of GDI systems, often in combination with turbo-charging and downsizing, offers significant benefits in terms of thermodynamic efficiency and pollutant formation control capabilities in peculiar operating conditions, such as part load and cold start [1,2,3]. The full achievement of the benefits potentially offered by this technology requires a deep knowledge and control capability of the complex in-cylinder phenomena following the fuel injection, which are basically regulated by the spray evolution and by its interaction with the surrounding air. To this end, the injection process must be investigated in several operating conditions, in order to extend as much as possible the stratified-charge strategy which requires the presence of a significant gradient for the local air/fuel ratio moving from the spark region to the combustion chamber walls.

In last years, GDI systems are evolving their control strategies in terms of mixture formation process, relying on the spray itself for the achievement of the correct combustion system operation (spray-guided systems). In order to improve the spray control capabilities, achieving a deep knowledge about the spray evolution is mandatory, along with developing accurate CFD tools to predict the possible interactions between the spray, the air flow field and the combustion chamber design. Among the experimental approaches, the measurement of the spray momentum flux, both according to the global and the local approaches, is receiving interest as it allows quantifying a physical quantity directly related to the spray-air mixing potential also in conditions in which more traditional optical techniques results are inadequate. Among the most diffused ones, Phase Doppler Anemometry operation is difficult in spray regions with excessive spray density, while imaging can hardly give a quantitative analysis of the flow distribution among the different jets.

In the same time, for GDI sprays a peculiar flow condition known as flash-boiling is being evaluated as a potential approach to improve the spray quality in terms of diffusion and atomization level [4,5,6,7,8]. Flash boiling is triggered by the fuel injection in an ambient in which the static pressure is below the fluid saturation pressure at the current fuel temperature. In flash boiling conditions, the abrupt fuel evaporation occurs not only at the liquid-gas interface but from the internal of the liquid phase, causing deep modifications in the spray evolution. These thermodynamic conditions can occur in part load operation for GDI engines, causing typically a shorter spray penetration and an improved atomization, with also enhanced spreading of the spray cone angle.

In the present paper, a deep analysis of the spray generated by a single-hole research GDI injector operating with *n*-heptane is presented and discussed. The working fluid was chosen in order to provide reliable experimental data that could be easily used for CFD tools tuning. Further, the single-hole design was chosen to avoid the jets collapsing in flash-boiling conditions, which prevents the clear analysis of the single spray in terms of shape and momentum flux. In a first part of the paper, the injection rate produced by the analyzed system operated at 50, 100 and 150 bar is presented. This measurement was intended to characterize the research injector hydraulic operation as a supporting tool for the spray analyses. The hydraulic analysis was carried out at ambient temperature conditions, with a relatively low counter pressure (5 bar) necessary to operate the proprietary Injection Analyzer used in this research. It is interesting to point out that with the currently available Injection Rate meters a significant counter pressure is required, preventing in this way the possibility to investigate the actual injection rate during flash boiling operation. In the second part of the paper, the results of an imaging campaign in a wide range of operating conditions in terms of fuel and injector nozzle temperature (respectively T_f and T_n) and test vessel counter pressure (P_v) are presented, discussing the effects of flash-boiling on the spray evolution in terms of tip penetration and global cone angle. Finally, in the same operating conditions tested by imaging, the spray global momentum and its distribution over a surface orthogonal to the spray main axis (spray local momentum) were investigated.

The global spray momentum flux measurement coupled with the injection rate measurement gives a deep insight of the spray evolution [12,13,14,15,16]. The global momentum flux is measured by an indirect method in which the spray-impinging force orthogonally onto a flat plate, named target, is evaluated. According to the momentum conservation equation, assuming steady state flow conditions are achieved, the force exerted by the spray onto the target equates the axial momentum flux issued from the nozzle. Moreover, with the assumption of uniform flow velocity at the nozzle exit, the effective discharge flow area and the flow exit velocity can be estimated allowing the evaluation of the in-nozzle cavitation intensity. The fully steady state flow condition attainment requires long energizing times which are quite far from the engine-like working condition; nevertheless, an adequate design of the momentum flux detection apparatus can minimize measurement errors allowing the momentum flux measurement also for short injection events [10]. As a complement of the global momentum analysis, a further improvement to better comprehend the internal flow structure has been accomplished [11]. According to this measurement technique, named local spray momentum, the momentum flux relevant to a small portion of the spray is analyzed independently of the rest of the jet, obtaining a momentum flux distribution inside the single spray structure.

Experimental Setup

The experimental campaign was carried out at the SprayLab of the University of Perugia, by means of a proprietary Injection Analyzer and self-developed momentum flux measurement bench. In order to characterize the spray shape evolution, an imaging system based on a high speed CMOS camera was also used.

In order to better focus on the injection process details in flash boiling conditions, a research single-hole injector IHP-293 from Magneti Marelli was used. This injector features a single, 0.2 mm diameter in-axis hole with a hole length-to-diameter ratio L/d= 3. The injector electrical driver used in the current tests is a Loccioni Mobility AEA 006 system, whereas the injector is fed by a static pressure generator Loccioni Mobility Thor system, with a fuel pressurization capability up to 900 bar. The test fuel is *n*-heptane (purity higher than 99.5%, physical properties reported in Table 1).

Table 1. *n*-heptane physical properties

Density [kg/m^3]		0.681 ÷ 0.687
Boiling Point [°C]	**@ 40 kPa** **@ 100 kPa** **@ 300 kPa**	69.65 98.25 140.35
Refractive Index		1.3836 ÷ 1.3916

Injection Analyzer

The UniPg Injection Analyzer (Figure 1) is a proprietary mass flow rate meter [19, 20] that allows both the injected volume and the injection rate time-history measurements in a given operating condition, defined by the injector energizing time (ET) and by the injection pressure. These measurements are resolved in the injector

actuation cycle, allowing a shot-to-shot analysis of both the injection rate profile and of the injected quantity. In case of multiple injections strategy, it is possible to evaluate the fluid volume relevant to each single event by measuring the respective injection rate curves.

The injection rate measurement is based on the Zeuch's Method, according to which the injection process takes place in a closed and constant volume chamber filled with the pressurized injected fuel. The fluid ΔV forced during the injection process by the injector into the chamber causes a rise ΔP of the vessel pressure P, which is proportional to ΔV according to the compressibility of the liquid β, indicated by its Bulk Modulus, and the chamber volume V_0.

$$\beta = V_0 \frac{\Delta P}{\Delta V} \tag{1}$$

Considering the density variations negligible during the injection process:

$$\frac{dm}{dt} = \rho \frac{V}{\beta} \frac{dP}{dt} \tag{2}$$

Therefore, the rate of injected mass can be considered proportional to the fuel density, to the chamber volume and to the rate of chamber pressure rise and inversely proportional to the fuel Bulk modulus.

Figure 1. UniPg Injector Analyzer.

Following each actuation cycle, a fast electro-valve is opened discharging the fuel and bringing the chamber pressure to the original base pressure before the next injection cycle starts. As the fluid Bulk Modulus is significantly influenced by both temperature and pressure, it can be hardly evaluated especially when performing tests with non-standard fuels. To achieve this task, the fuel discharged from the instrument chamber flows through a Coriolis mass flow meter (Siemens Sitrans CF 2100) to measure the mean injected mass and the fuel density, so to ensure a continuous system calibration in the actual operating conditions. After a proper thermal stabilization in each operating condition, the acquisition procedure is repeated for some hundreds of consecutive injection cycles in order to allow a statistically significant analysis of the process mean characteristics and of its shot-to-shot dispersion in terms of injection rate and injected quantity. The bench control system is developed in LabVIEW™ environment and it is structured on different levels to manage the injector logical commands, data acquisition and analysis tasks.

Imaging Apparatus

The spray evolution is analyzed by means of a high speed camera (Vision Research MIRO 310 M) synchronized with the injector actuation and operated at 20 kframe/s, with 1 μs exposure time. High power leds are used as lighting system, arranged so as to have the high speed camera and the leds at the same side of the lighted spray.

Both imaging and momentum test are performed in an ambient temperature test vessel designed to withstand sub-atmospheric (minimum P_v= 30 kPa) and pressurized (maximum P_v= 1200 kPa) operating conditions. The injector is mounted on an electrically heated fixture (Figure 2); the temperature of the metal shield around the nozzle T_n is the control parameter of the fixture temperature regulation system. The fuel is supplied by the Thor system via a stilling volume (290 cc) just upstream the injector that is used as fuel heat exchanger; for this apparatus the fuel temperature at the injector inlet T_f is used as feedback quantity for the heating system, while the heating element temperature inside the stilling volume is detected for safety purpose.

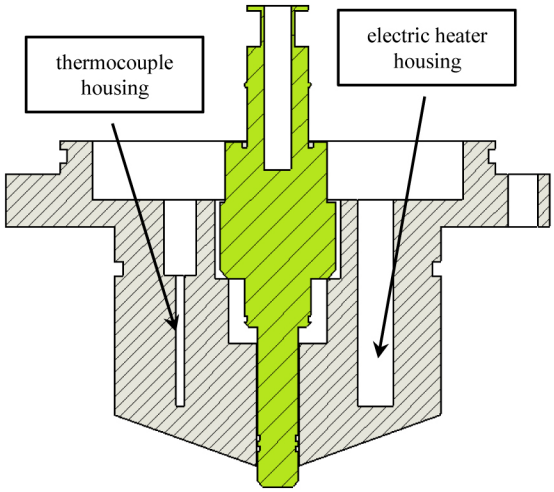

Figure 2. Heated injector fixture.

The spray images acquired by the high speed camera are off-line analyzed by means of a self-developed automated procedure developed in LabVIEW Vision™ environment, allowing the construction of the spray tip penetration and cone angle curves. To this end, single frames are extracted from the high speed videos and binarized in order to locate the spray structure. The resulting 2-bit images are then processed in order to compute the spray tip penetration and global cone angle. The tip penetration is defined as

the distance between the nozzle hole and the most advanced spray tip portion, while the spray cone angle includes the spray structure for its entire tip penetration length. More details about the image analysis procedure are reported in [17,18,19].

Momentum Flux Measurement

The spray global momentum flux measurement is based on the detection of the force exerted by the spray when it impacts a flat surface (target) positioned orthogonally to the spray main axis. For this application, the force is measured by means of a piezo-electric sensor (Kistler 9215) coupled with its charge amplifier (Kistler 5011). A 12 mm diameter target is screwed on the sensor and the so-build sensing device is positioned by means of a 3-axis Cartesian coordinate system, assembled by three OWIS optical guides moved by stepper motors (1/200 mm/step). The positioning system is designed to operate with vessel pressure up to pressure of 60 bar, with travel ranges ± 14 mm in both X, Y- axis and 65 mm along the Z-axis coincident with the injector axis. The least vertical distance for the global momentum flux measurement is 5 mm, and 10 mm in the local momentum measurement test (Figure 3). The positioning system, injector control and data acquisition tasks were carried out by two NI DAQ boards (PCI 6221 and USB6008) controlled by a self-developed software (NI LabVIEW™).

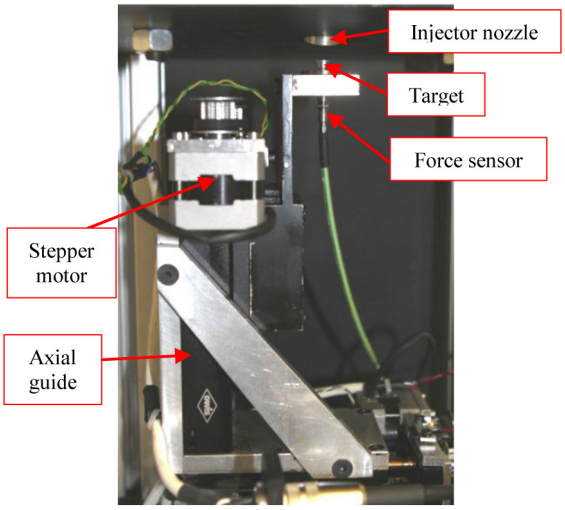

Figure 3. Momentum flux instrument and positioning system.

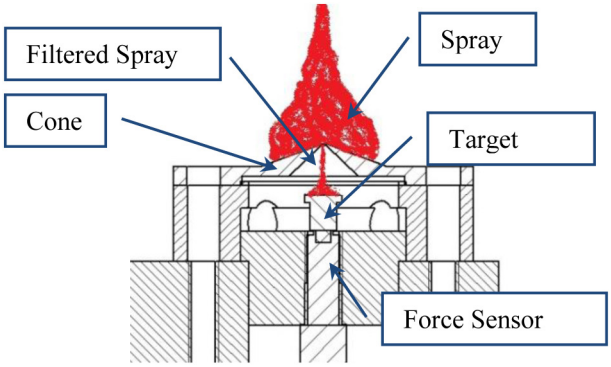

Figure 4. Conical adapter for local momentum flux measurement.

In order to accomplish the local momentum analysis, the impact force measurement must be relevant to small portions of the spray structure. The analyzed spray portion is studied in the same way of the global momentum flux test except that the spray is mechanically filtered in such a way to deflect the non-required portions. The mechanical filter should be as less intrusive as possible, providing a non-disturbed, free jet momentum flux measurements. To isolate a spray flow tube, the operation of different mechanical filters was investigated experimentally and by a CFD analysis [11], suggesting the use of a filter based on a small-holed cone-shaped device: in Figure 4 the principle and the general fixture shape are reported [21]. Underneath the target the same piezoelectric force-sensor used for global momentum measurement captures the impact force. The measurement is repeated over a grid of positions (127 in this research) covering a virtual map whose integration over a surface normal to the spray axis ideally equates the global momentum flux. Dissipative phenomena occurring with the spray-mechanical filter interaction possibly cause the integrated local momentum not to reach the corresponding global momentum measurement, with a typical 8 to 12 % discrepancy. It is noteworthy to mention that the target for both global and local momentum flux tests should accommodate the spray whether it is the whole jet or a portion of it. The target size should be larger than the impinged spray in order to ensure a correct spray deviation, but not too wide to avoid the noise which can affect the resultant momentum measured value [10].

Results and Discussion

The hydraulic characterization of the research 1-hole injector was carried out by means of the UniPG Injection Analyzer. The injector was actuated with the current profile depicted in Figure 5, where some of the used ETs are reported. The obtained results in terms of mean injected volume for P_{inj} =50 bar, 100 bar and 150 bar are reported in Figure 6. In the (a) plot, the mean injected volume per shot evaluated over a 300 consecutive shots basis is reported as a function of the injector actuation command duration (EMI curve); in Figure 6 (b) the injected volume shot-to-shot dispersion over the same 300 shots is evaluated in terms of CoV (Coefficient of Variation). As can be seen, the EMI curves evidence a net slope change confirming the typical two-region operation of a GDI injector: ballistic and linear. For small ETs pertaining to ballistic operation, in which the needle does not attain the fully raised position, the EMI curve is typically non-linear and it is characterized by a high mean slope and by a relatively high injected volume shot-to-shot dispersion. On the contrary, for higher ETs the EMI curve is well-linear; further, both its slope and the shot-to-shot dispersion are noticeably reduced with respect to the ballistic zone: in the present case, the CoV in the ballistic operation ranges between 1 % and 8%, while it is below 1% in the linear operation zone. As can be seen, the minimum ET required for the injector to open slightly increases with the supply pressure, along with the ET at which the transition from ballistic to linear operation is achieved: from 300 µs @ P_{inj}=50 bar to 330 µs @ P_{inj}=150 bar.

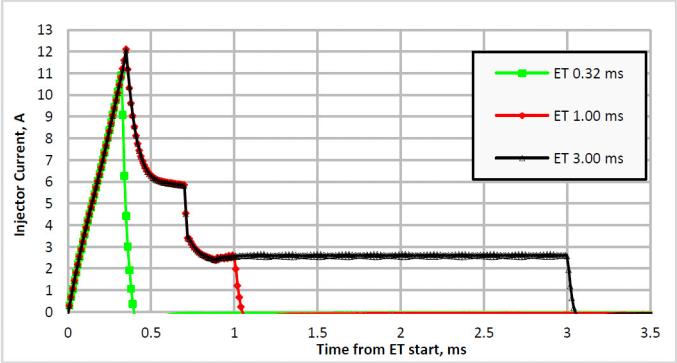

Figure 5. Injector current profile.

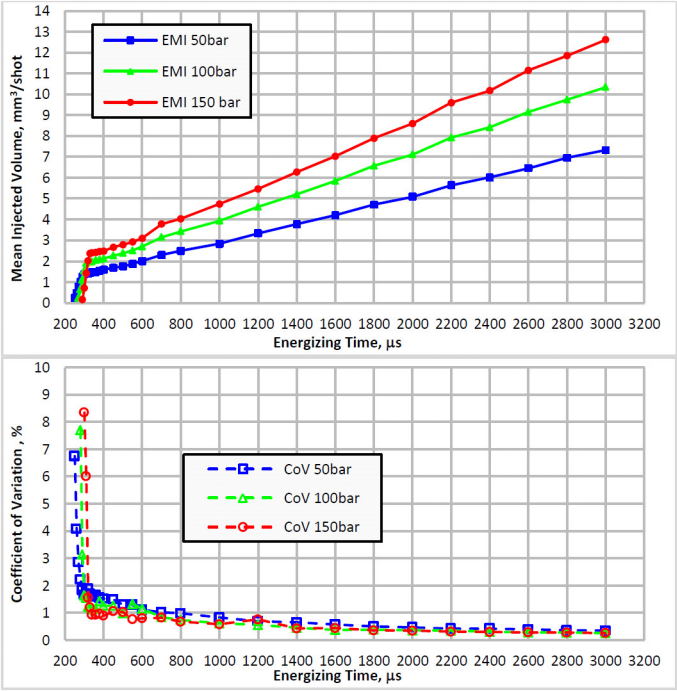

Figure 6. (a) Mean injected volume, Pinj 50, 100 and 150 bar. (b) Shot-to-shot coefficient of variation.

In Figure 7, the mean injection rate (IR) curves for ET= 0.4 ms and 3 ms are reported for the three examined injection pressure levels (EVI curves). These mean IRs are computed over the same 300 consecutive injection events used to determine the EMI curves (Figure 6). For all the pressure levels, the reported profiles are pertaining to the linear operation mode of the injector. At both P_{inj}=50 bar and P_{inj}=100 bar, the injection rate profiles evidence a smooth operation, with a fast opening transient and very moderate injection rate oscillations in the full needle lift operation phase. At P_{inj}=150 bar, a short injection rate peak is observed at the end of the opening transient, possibly caused by the needle hit on its stop. The injection process end is net for all the operating conditions, without any evidence of bouncing phenomena and with small residual oscillations in the rate signal (within ± 0.2 mm³/ms), that could be due to mechanical vibrations of the injector-instrument assembly.

In Figure 7 (b) a zoom of the same injection rate plots allows to appreciate the effect of increasing the supply pressure on the injector opening phase with unchanged actuation current strategy. Following the application of the current to the solenoid (timing 0 in the plot), the first observed phenomenon is the IR signal crossing zero towards negative values (around 0.2 ms), possibly associated with a backflow from the Injection Analyzer measuring chamber towards the nozzle as a consequence of the first needle rising movement. Consequently, negative values of the cumulative injected volume are obtained (Figure 7 (b)); a similar behavior was already observed for Diesel systems [20]. Following this scheme, the actual start of injection can be computed as the timing in which the time-integral of the injection rate (injected volume) crosses zero towards positive values, around 0.3 ms from ET start for the P_{inj}=100 bar condition in Figure 7 (b). This injection start timing is in good agreement with the spray imaging results (see Figure 9). The fluid pressure inside the injector body acts against the needle rise, hence increasing P_{inj} delays the timing at which the IR profile crosses zero towards positive values (hydraulic injection start) and consequently the actual injection start. Once the effective flow section between the needle and its seat has started to grow, clearly a higher injection pressure results in a higher instantaneous flow rate detected by the Injection Analyzer. As a consequence, the minimum ET value to obtain the injector actual opening (a measured non-null injected quantity) is typically lower for lower injection pressure levels and the transition from ballistic to linear operation mode is shifted towards higher ETs at higher injection pressure level. At full needle lift, in steady flow conditions, the measured injection flow rate is proportional to the square root of the pressure differential between the nozzle and the injection analyzer chamber, hence it increases for higher injector pressure, as shown in Figure 7 (a).

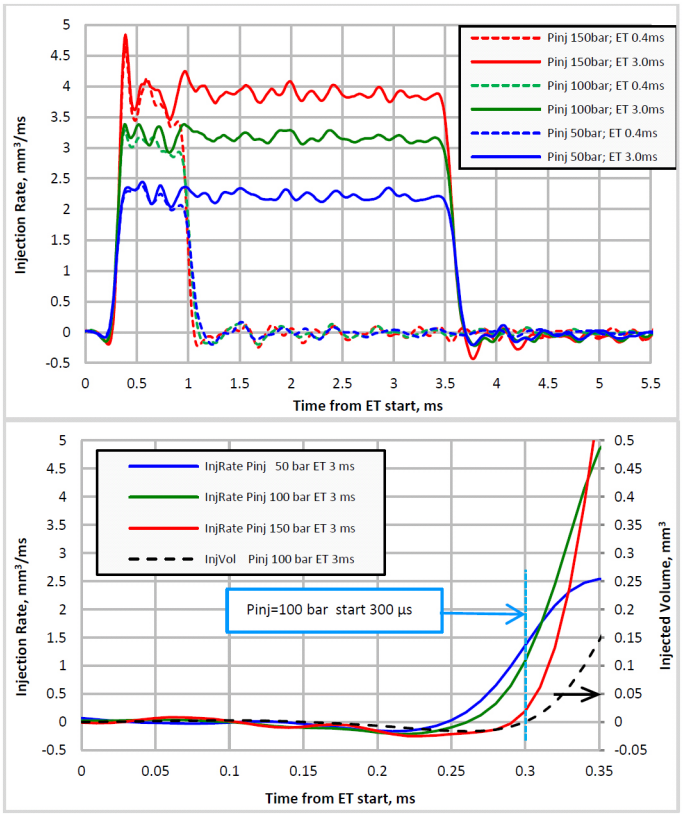

Figure 7. (a) Injection rate profiles for P_{inj}=50 bar, P_{inj}=100 bar and P_{inj}=150 bar. (b) Injected volume for P_{inj}=100 bar, ET=3 ms.

Spray Imaging

In order to obtain basic information about the spray development in different operating conditions in terms of injection pressure, fluid and injector temperature and vessel pressure, an experimental campaign was set-up based on high speed imaging. The test plan reported in Table 2 was executed, composed of nine operating conditions per injection pressure level. In Table 2, for each operating condition the corresponding value of Air-to-Saturation Pressure Ratio - AtSPR for *n*-heptane is reported. AtSPR can be considered an efficient indicator of the spray tendency to experience flash-boiling.

The effect of the different AtSPR values on the spray development can be clearly perceived from the pictures reported in Figure 8; here, the spray global structure at 0.5 ms after the ET start for the P_{inj}=100 bar conditions can be observed, while in the following Figure 9 and Figure 10 the spray tip penetration and global angle trends (mean over 30 injection events) are reported for the entire set of operating conditions. Further, in the same Figure 9 and Figure 10, the obtained tip penetration and cone angle standard deviations are reported.

Table 2. Test Plan and AtSPR

		Inj. Fixture & Fuel Temperature [°C]		
		30	90	120
Vessel Pressure [kPa]	40	8.47	0.51	0.22
	101	21.38	1.28	0.55
	303	64.16	3.85	1.65

As reported by Xu *et al* [4], three ranges for AtSPR can be defined to evaluate the tendency to flash-boiling (Table 3).

Table 3. AtSPR ranges for flash-boiling.

AtSPR > 1	No Flash-Boiling
0.3 < AtSPR < 1	Transition Zone
AtSPR < 0.3	Full Flash-Boiling

As can be observed in Figure 8, the spray structure is completely different depending on the AtSPR value, with a narrow cone angle at ambient temperature conditions regardless the vessel pressure. As the fuel and nozzle temperature (T_f and T_n respectively) are increased and the vessel pressure is kept sub-atmospheric (first line in Figure 8) so to have AtSPR values below 1, significant changes in the spray structure can be observed, with increased cone angle and progressively reduced spray tip penetration. Finally, in the T_n=120 °C, and P_v =40 kPa, full flash boiling conditions are attained (AtSPR=0.22). In these conditions, the spray cone angle is dramatically increased, the spray length is reduced and wide recirculating zones are present on the spray tip front. Further, the spray seems to be composed by finely atomized drops, suggesting the substantial onset of flash boiling-induced ligaments breakup phenomena immediately downstream the nozzle exit. Conversely, in atmospheric pressure conditions (second row line in Figure 8) the same increase in the fuel and nozzle temperature does not allow the achievement of full flash boiling conditions and only a partial modification of the spray structure is obtained. In pressurized conditions (303 kPa, third line in Figure 8) the spray structure is almost un-affected by the fuel and nozzle temperature, with only minor spray tip structure variations.

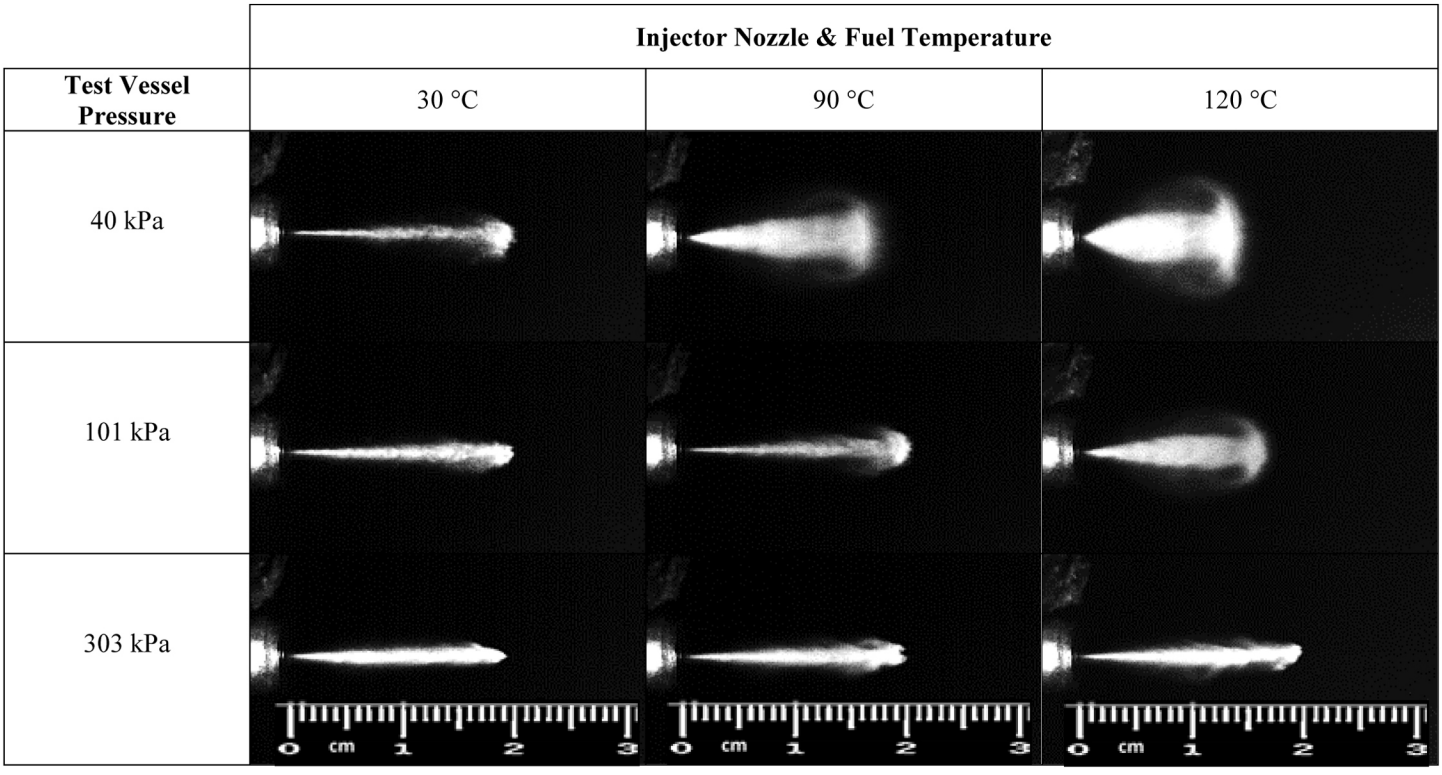

Figure 8. Spray global structure, P_{inj} 100 bar - Delay 0.5 ms from ET start.

The vessel pressure and nozzle temperature effect on the spray structure can be quantified in terms of standard indexes such as tip penetration and cone angles. As can be appreciated in Figure 9 (a), in low temperature conditions the increase of the vessel pressure causes the spray front to slow down as a result of the increased aerodynamic drag exerted on the spray droplets. When comparing the penetration curves at T_f and T_n=90°C (Figure 9 (b)), it is evident that if the flash boiling phenomenon is not triggered (P_v =101 and 303 kPa) the pressure increase effect is very similar to what is observed at low temperature. Conversely, the reduction of the vessel pressure to 40 kPa provokes partial flash boiling at this temperature, causing a dramatic spray tip slowing instead of a penetration increase. In high temperature conditions (T_f and T_n=120°C, Figure 9 (c)), at P_v =101 kPa flash boiling conditions are partially established (AtSPR= 0.55) and the spray structure is significantly altered from its standard, low temperature evolution, with a significantly reduced penetration length. In this temperture conditions, the maximum penetration is obtained in high vessel pressure conditions, in which the tip penetration potential is only partially reduced with respect to the equal vessel pressure and low temperature condition, possibly as an effect of the improved evaporation mechanism.

The spray global angle trends as measured in the nine operating conditions at P_{inj} 100 bar are reported in Figure 10. In low temperature conditions, as expected, the effect of the vessel pressure on the spray cone angle is relatively moderate (Figure 10 (a)), with a higher vessel pressure causing a higher cone angle in steady flow conditions. At P_v = 303 kPa the measured spray cone angle at 1.0 ms after the ET start is about 7 deg *vs.* about 3 deg with P_v = 40 kPa. Moreover, at P_v = 40 kPa the internal spray structure seems to be composed of a very narrow liquid jet emerging from the nozzle and by a relatively large plume on its tip (see Figure 8). In pressurized conditions (P_v = 303 kPa) the spray structure appears to be more compact and solid, with intermediate characteristics at P_v= 101 kPa. Increasing the fuel and nozzle temperature to 90 °C (Figure 10 (b)) causes the P_v= 40 kPa global angle plot to be entirely shifted towads higher values, well above the plots pertaining to the P_v = 101 kPa and P_v= 303 kPa conditions. As observed for the penetration analysis, the flash boiling onset is almost complete for this P_v = 40 kPa operating condition, causing a dramatic alteration of the spray structure. For higher vessel pressure levels at 90 °C, the observed global angle values are very similar to the corresponding low temperature ones, while it is interesting to point out that the global spray structure at P_v = 101 kPa, 90 °C is very similar to the one observed at P_v = 40 kPa, T_n=30°C and it is composed of a narrow stem and a well defined plume on its tip. This seems to suggest that even in conditions in which AtSPR is relatively far from the above mentioned 0.3 threshold, the combined effect on the spray structure exerted by vessel pressure and nozzle temperature can be significant.

Finally, when the T_f and T_n=120°C conditions are considered, the spray global angle is strongly affected by the vessel pressure level: if the full flash boiling condition is completely achieved (P_v = 40 kPa), at 1 ms from the ET start the observed cone angle values is 17.5 deg *vs.* 2.9 deg obtained in low temperature conditions. Also in partial flash boiling conditions (P_v = 101 kPa, T_f and T_n=120°C) the spray cone angle increase is significant approaching 13 deg as final value being about 5 deg with T_f and T_n=90°C. Conversely, when the AtSPR value is far from triggering flash boiling (P_v = 303 kPa), the final spray cone angle value is substantially unaffected by the fuel and nozzle temperature, being in any case around 7 deg.

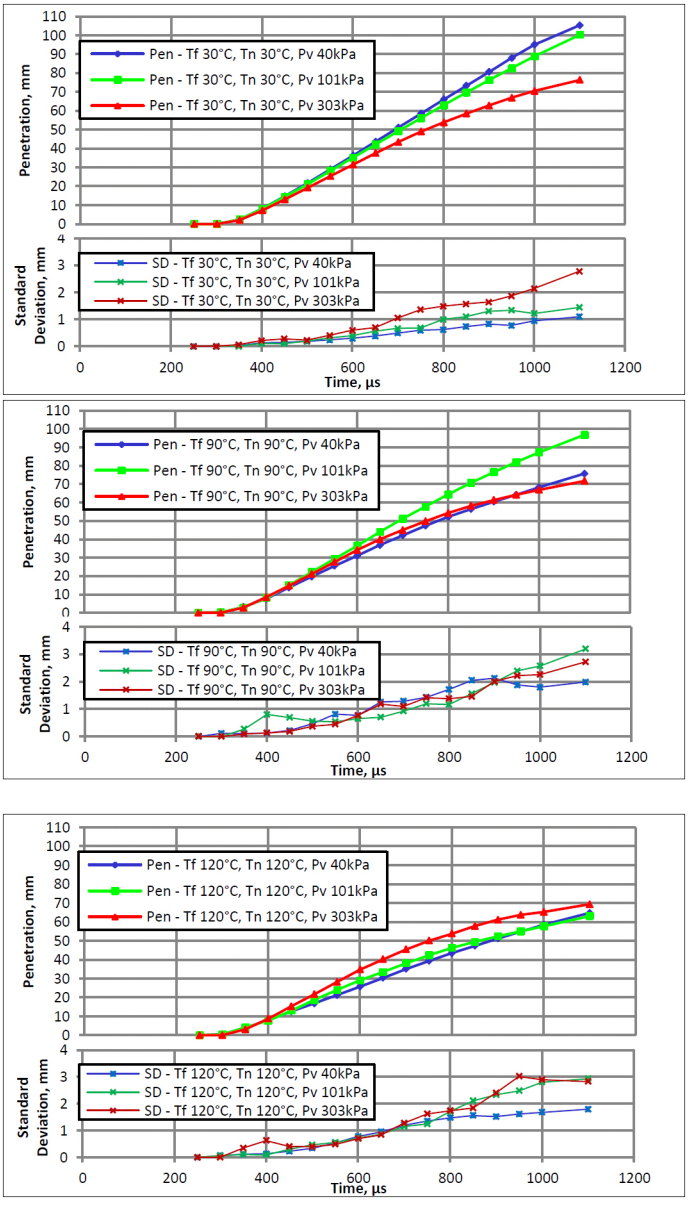

Figure 9. Spray tip penetration with standard deviation for P_{inj} 100 bar, ET = 1.5 ms; (a) T_f , T_n=30°C; (b) T_f, T_n=90°C; (c) T_f , T_n=120°C.

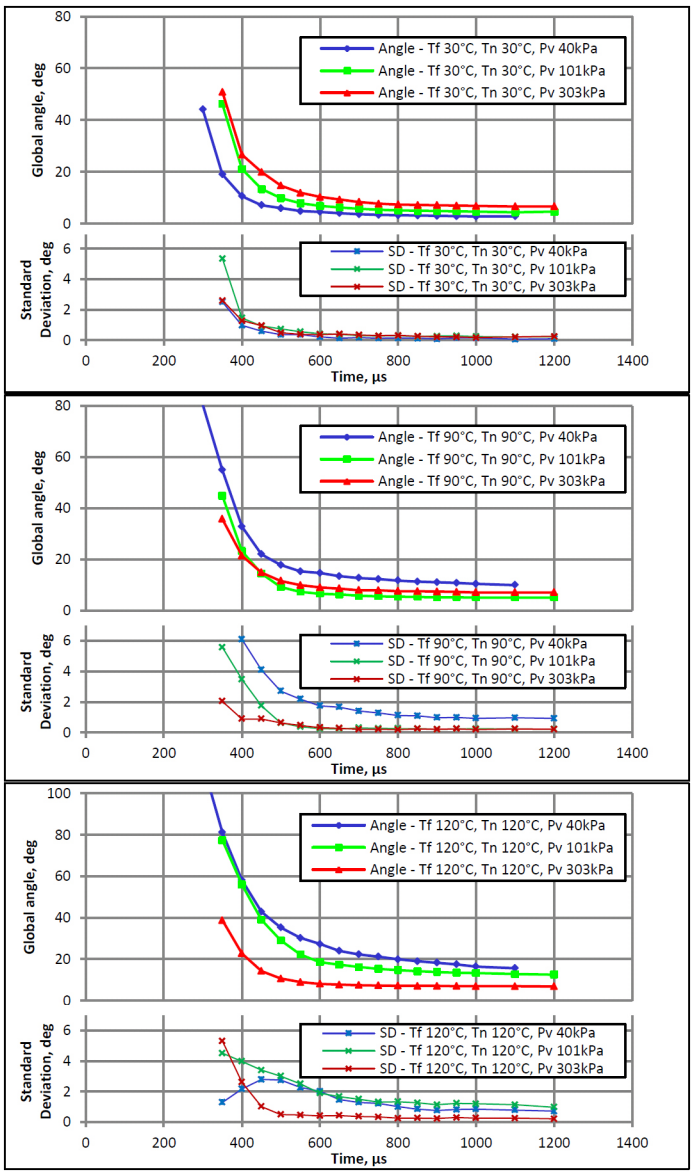

Figure 10. Spray cone angle with standard deviation for P_{inj} 100 bar, ET=1.5 ms; (a) T_f, T_n=30°C; (b) T_f, T_n=90°C; (c) T_f, T_n=120°C.

Spray Momentum Flux Measurement

Despite imaging is a powerful tool to analyze the effects of flash boiling phenomenon on the spray shape evolution, it cannot assit in investigating the hydraulics of the injection process. To this end, the global momentum flux measurement is an interesting approach that can be used to analyze the eventual effects exerted in flash-boiling by the abrupt fuel transition from liquid to vapor phase on the discharge process from the nozzle. Further, the analysis of the momentum flux distribution over a surface orthogonal to the spray main axis (spray local momentum analysis) can support in quantitatively evaluate the flash-boiling effect on the spray internal structure with respect to its evolution in standard conditions. The comparison of the obtained local momentum flux maps with the results of CFD computations can help in understanding both the in-nozzle and downstream the nozzle flow characteristics.

In Figure 11 the time profiles of the spray impact force on the target are reported (mean over 30 consecutive events) for the injector operated at P_{inj}=100 bar, ET=1.5 ms in ambient pressure (P_v= 101 kPa) and low temperature test vessel conditions, with the impact force measured at different nozzle-target Z distances from 5 to 40 mm. As can be seen, the impact force onset is relatively sharp for all the Z distances, without significant signal oscillations before the impact force detection start. The transition to the steady state flow condition, during which the flow is orthogonally deviated by the spray, evidences a local peak-and-valley structure. As discussed in [9-10], this behaviour can be related to the presence of a transient toroidal vortex around the spray tip during the first impact on the target. During this transient phenomenon, the target perceives the local depression associated with the toroidal vortex until this flow structure moves radially towards the target periphery. This behaviour is particularly evident for Z=5 mm, for which the 12 mm diameter target is probably too large, while for higher distances this transient interaction between the target and the spray seems to affect the force signal to a lesser extent.

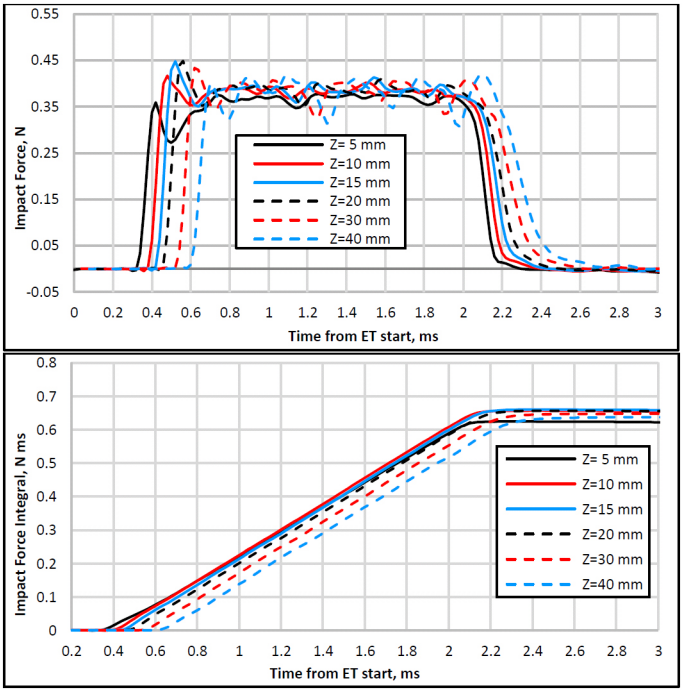

Figure 11. Global momentum profiles (a) and momentum time-integral (b) for P_{inj}=100 bar, ET=1.5 ms at different Z nozzle-target distance. P_v= 101 kPa, T_f, T_n=30°C.

As can be seen in Figure 11 (a), the impact force level is not significantly affected by the target distance during the steady state flow period. In fact, the actual spray structure at a given distance from the nozzle is not signficant in terms of global momentum flux since both the liquid and gaseous phases contributions are accounted by the impact measurement method. A peculiar behaviour was observed in terms of impact force profile for Z=5 mm, with a lower mean value probably due to a non-regular flow deviation by the target to the orthogonal direction. For higher distances, the observed mean values are very similar, with the force profiles evidencing low frequency oscillations for the longer distances, possibly due to the non-homogeneous flow structure for the completely developed spray,

also evidenced by imaging. The time-integral of the impact force profiles at 3 ms (Figure 11 (b)) are almost identical for Z distances from 10 to 40 mm, while a slighlty lower value was obtained for Z=5 mm confirming an abnormal target behaviour at this distance. The target distance Z=10 mm will be considered in the following analyis.

In Figure 12, 30 consecutive records of the spray impact force profile are reported for 10 mm nozzle-target distance. As can be seen, the repeatability of the measure is satisfactory. As a global indication of the measured shot-to-shot dispersion, the impact force time-integral CoV was computed; the results are reported in Table 4. The CoV is lower than 0.5% for all the analyzed distances, with the maximum value obtained for the longer nozzle-target gap (Z=40 mm), where possibly some peripheric portions of the spray may begin to escape the target.

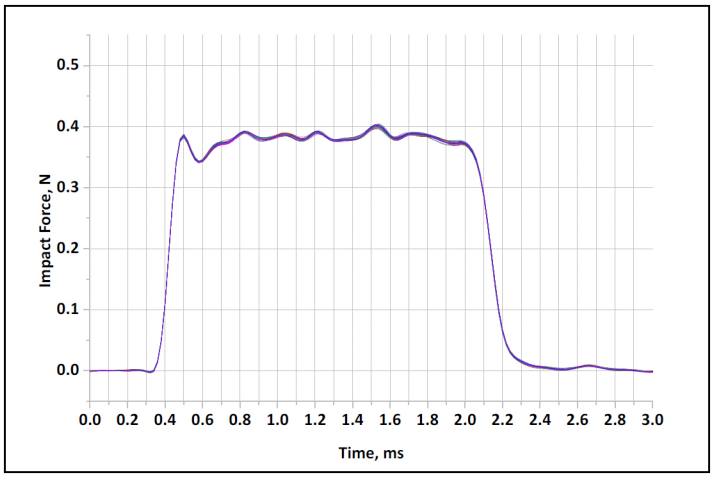

Figure 12. Global momentum profiles of 30 consecutive injection events for P_{inj}=100 bar, ET=1.5 ms, Z =10 mm, P_v= 101 kPa, T_f, T_n=30°C.

In Figure 13 a direct comparison between the measured injection rate and momentum flux profiles is reported for P_{inj}=100 bar, ET=3.0 ms, T_f, T_n=30°C operating condition. The injection rate was measured by the Injection Analyzer with a 5 bar counter-pressure, while the momentum flux was detected with a P_v= 303 kPa vessel pressure. A time gap between the two signals onset is normally present and it is due to the time required by the spray tip to travel from the nozzle to the target. Analyzing the injection rate profiles in Figure 7 (b), the injection start timing was assumed to be 300 µs from the ET start for P_{inj}=100 bar, as also confirmed by imaging; the injection start timing is not affected by the ET value. In the considered condition, assuming a mean spray tip velocity of 120 m/s (evaluated from the penetration curve slope) the resulting travel time is around 80 µs. Globally, the spray tip is presumed to approach the target at around 380 µs from the ET start, in a good agreement with the first momentum signal onset reported in Figure 13. In the closing transient, the impact force curve seems to follow the injection rate trend with a delay similar to the above described travel time from the nozzle to the target. Further, the impact force time-profile evidences a slope change in its final part that seems to be correlated to the injection rate end (about 3.7 ms). The following impact force signal transient, slowly approaching zero, is probably caused by the tail of the spray impacting at low velocity on the target. With higher nozzle-target distances the described impact force slope change is progressively less evident, possibly due to the less compact spray structure.

Table 4. Impact force time-integral, mean value and CoV. P_{inj}=100 bar, ET=1.5 ms, P_v=101 kPa, T_f, T_n=30°C.

	Target-Nozzle distance, mm	Force Integral mean, N*ms	Force Integral CoV, %
Impact force time-integral	5	0.634	0.291
	10	0.658	0.299
	15	0.659	0.167
	20	0.657	0.256
	30	0.649	0.238
	40	0.641	0.441

In Figure 14 the comparison of the global momentum flux time-profiles obtained with P_{inj}=50 bar, 100 bar and 150 bar at ambient counter pressure and low temperature conditions is reported. As can be seen, no significant differences in the signal onset timing can be observed; as above discussed (Figure 7 (b)), with high rail pressure the injection start is slightly delayed but the later IR slope is higher, possibly resulting in similar timing for the spray approach to the target. The effect of a higher IR slope with higher injection pressure is also appreciable in terms of a higher impact force slope in Figure 14. Parallely the end of the injection process does not seem to be influenced by the injection pressure level as alreay observed by the Injection Analyzer (Figure 7 (a)). As expected, in steady flow conditions in the 0.8 ms to 1.8 ms time-window, the mean impact force values at the different injection pressure levels (0.189 N, 0.385 N and 0.582 N for 50bar, 100 bar and 150 bar respectively) seem to be correctly correlated with the corresponding pressure difference between the nozzle and the vessel pressure. Given the easily predictable effect of the injection pressure level, in the following analyses only the P_{inj}=100 bar data will be shown for the sake of brevity.

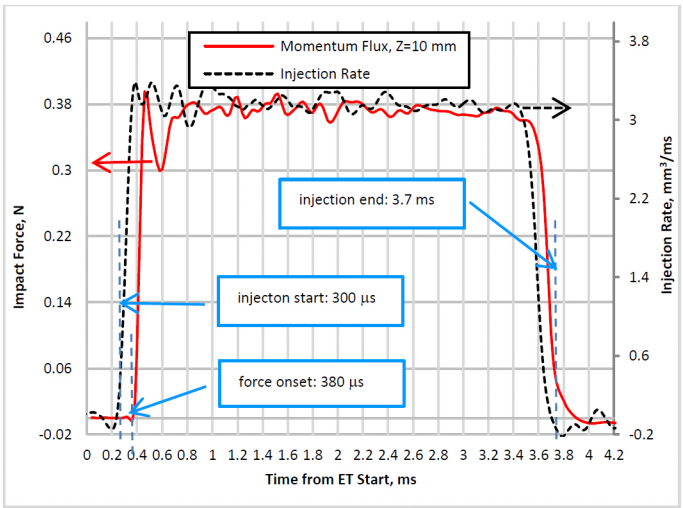

Figure 13. Injection rate and momentum flux for P_{inj}=100 bar, ET=3.0 ms. T_f, T_n=30°C.

In Figure 15 the global momentum time-hystories obtained for the nine considered operating conditions with P_{inj}= 100 bar and ET=1.5 ms are reported for a direct evaluation of the vessel pressure effect at

the different fuel and nozzle temperature levels 30 °C, 90°C and 120°C. In Figure 16 the same results are plotted evidencing the temperature level effect in terms of global momentum flux.

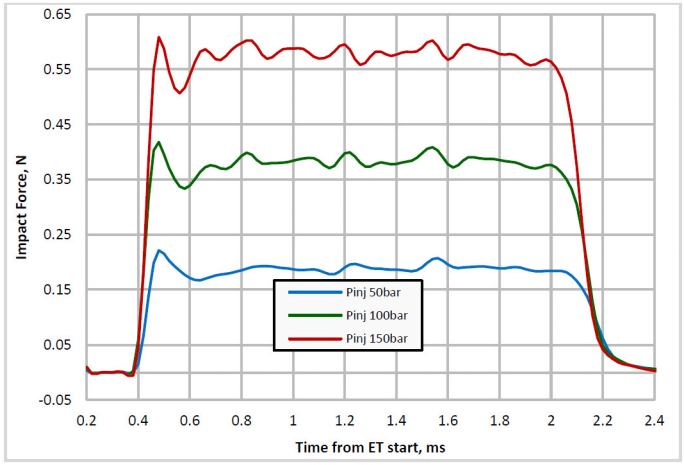

Figure 14. Momentum flux for P_{inj}=50 bar, 100 bar and 150 bar. ET=1.5 ms, P_v= 101 kPa, T_f, T_n=30°C.

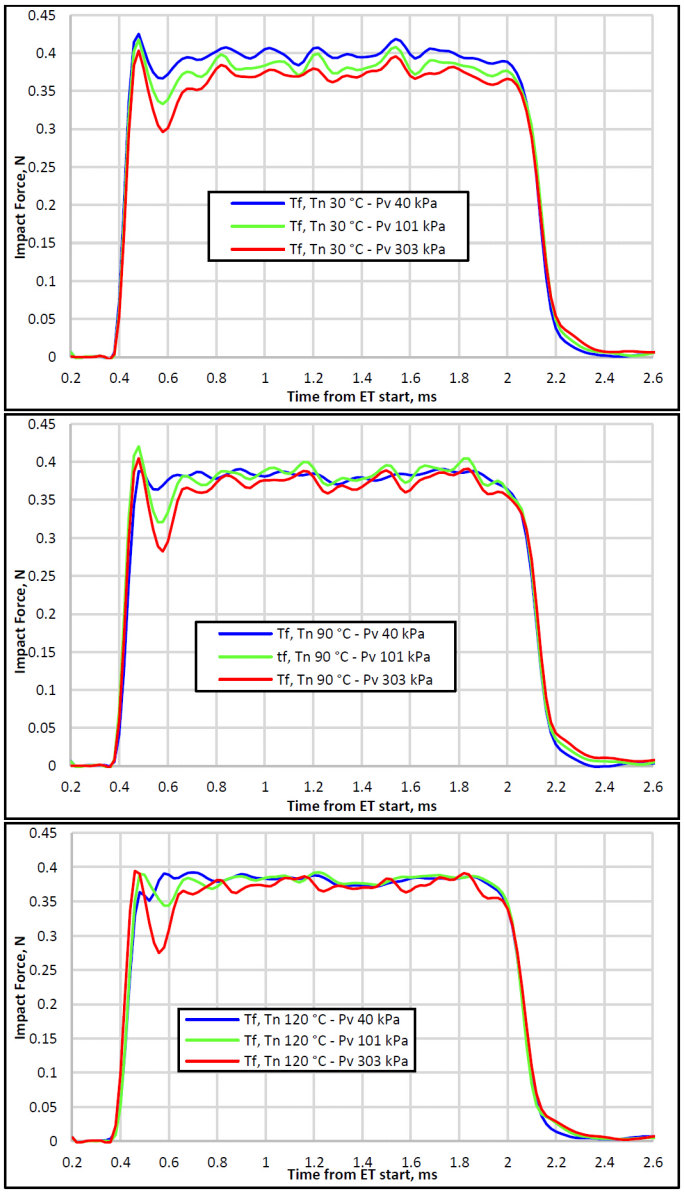

Figure 15. Global momentum flux time-history, P_{inj}=100 bar, ET=1.5 ms; (a) T_f, T_n=30°C; (b) T_f, T_n=90°C; (c) T_f, T_n=120°C.

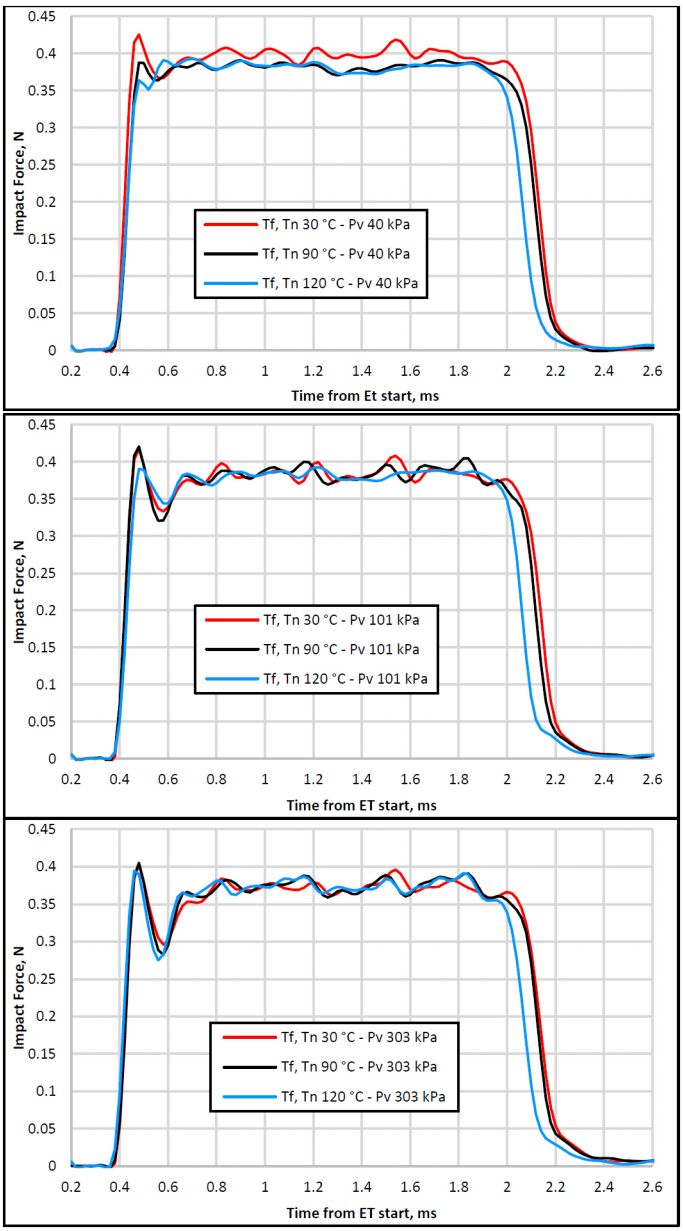

Figure 16. Global momentum flux time-history, P_{inj} 100 bar, ET= 1.5 ms; (a) T_f, T_n=30°C; (b) T_f, T_n=90°C; (c) T_f, T_n=120°C.

As can be seen in Figure 15 (a), in low temperature conditions the mean momentum flux measured in the steady flow phase of the injection process (from 0.8 ms to 1.8 ms from ET start) is affected by the vessel pressure level. In detail, when reducing the vessel pressure the relative rise of mean impact force is higher than the correponding ΔP increase, suggesting a possible non orthogonal deviation of the spray after the interaction with the target (spray partial bounce) in these non-flash boiling operating conditions (P_v= 40 kPa, T_f, T_n=30°C) possibly due to the very narrow spray structure. Increasing the fuel and nozzle temperature to 90 °C and 120 °C, the impact force

mean values obtained at different counter pressure levels are more similar each other, with in any case lower values pertaining to the P_v= 303 kPa conditions. Further, in partial or full flash boiling conditions (P_v= 40 kPa in Figure 15 (b), P_v= 40 kPa and 101 kPa in Figure 15 (c)) the impact force oscillations are significantly less evident, suggesting the development of a more uniform spray structure, as also evident in Figure 8.

The analysis of the same results reported in Figure 16 allows to evidence that the fuel and nozzle temperature level has no significant effect in terms of mean global momentum flux in the steady flow conditions for the vessel pressure levels 101 kPa and 303 kPa.

With sub-atmospheric vessel pressure conditions, the measured impact force at low temperature was higher as already observed. Conversely, temperature seems to markedly influence the closing transient phase, causing an evident reduction of the injection duration that was confirmed by imaging. Increasing the fuel and nozzle temperature to 120 °C, the momentum flux slope in the injector closing phase does not seem to be altered, rather the timing in which the needle starts to move downward seems to be influenced. Further, the mean momentum flux in the steady flow condition does not seem to be affected by the temperature level. According to these evidences, the observed temperature-induced injection shortening effect does not seem to be due to fluid-dynamic differences in the discharge process (possibly given by changed fluid density or viscosity), but rather it seems to be caused by a different behavior of the injector electromechanical parts. The further evidence that this phenomenon takes place also at the higher counter pressure conditions, in which flash boiling is not triggered, seems to confirm that the flash boiling phenomenon does not alter the spray global momentum flux, at least in the analyzed operating conditions.

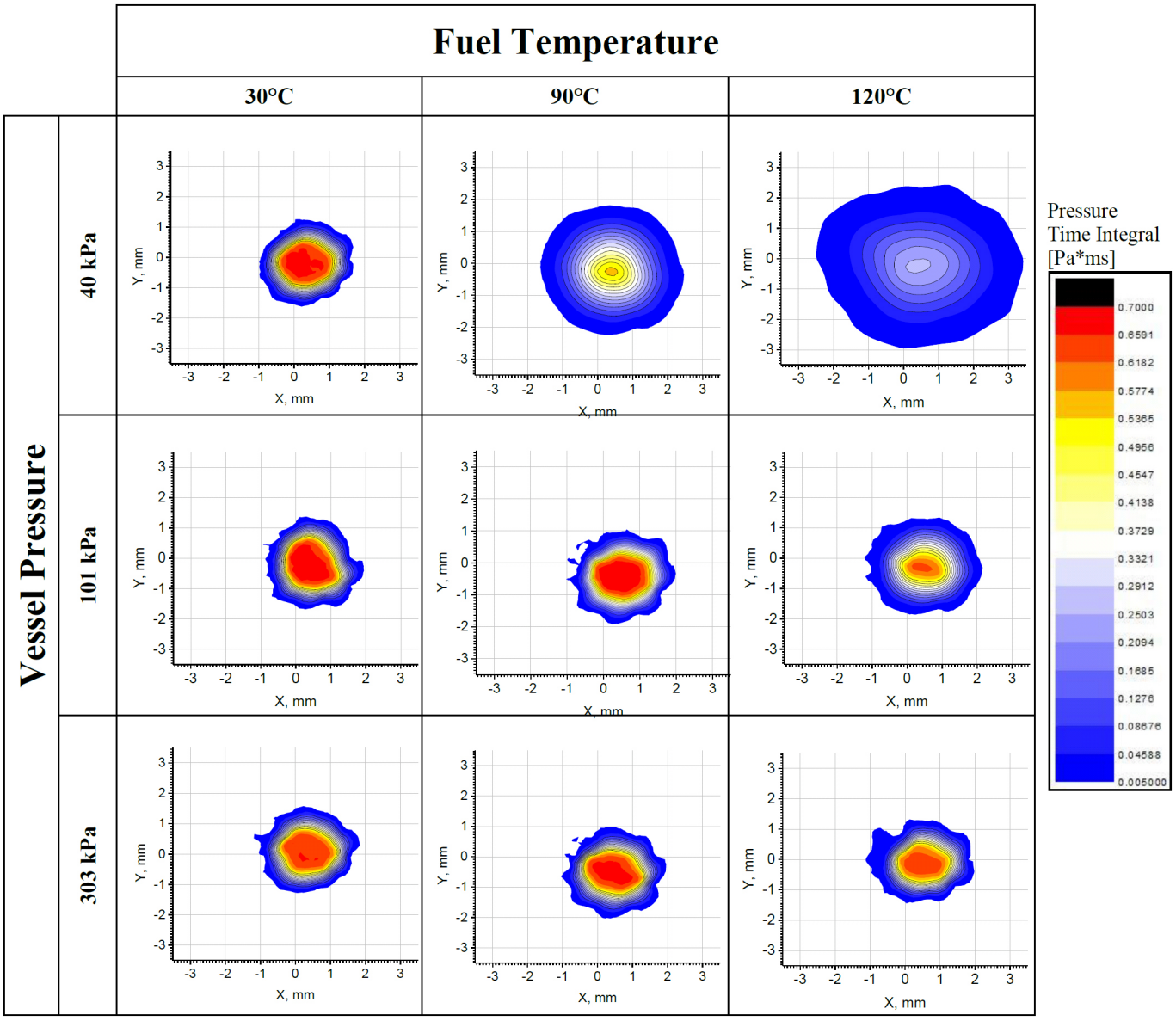

Figure 17. Momentum maps in integral form; P_{inj} 100 bar, ET= 1.5 ms. Nozzle-target distance Z=10 mm

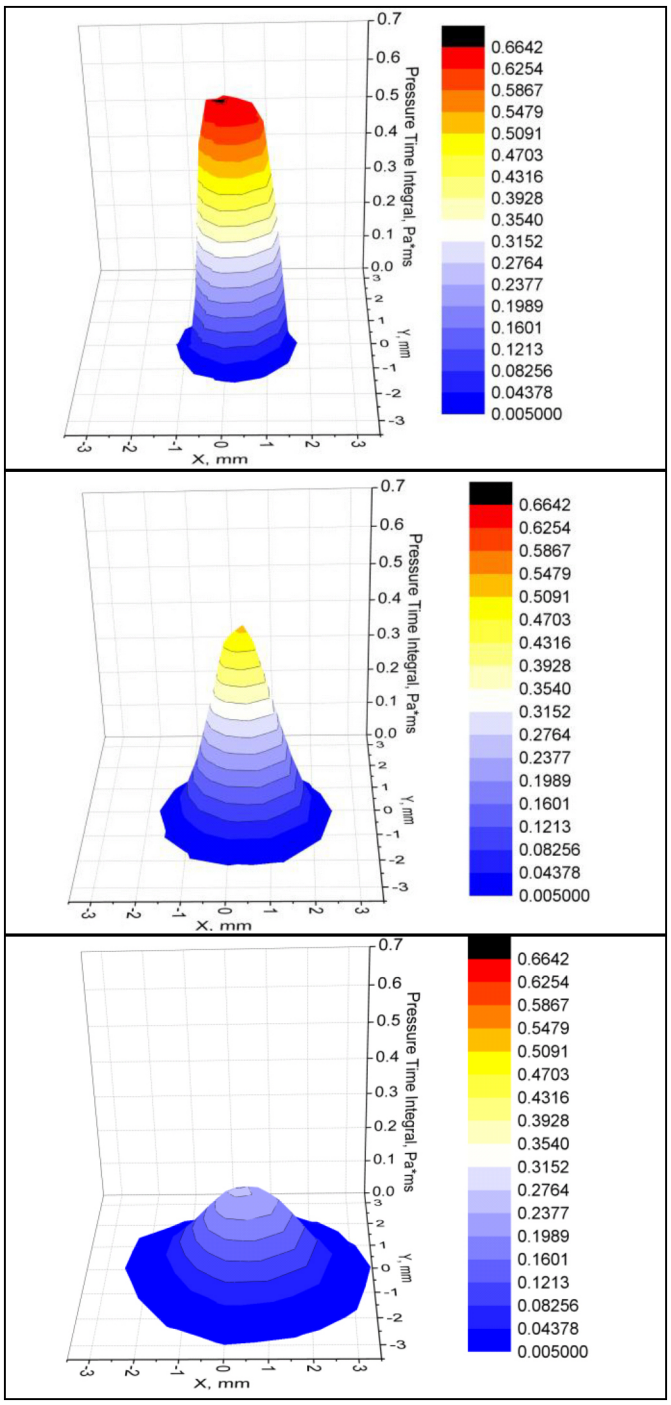

Figure 18. Comparison of 3D momentum maps (integral form). P_{inj} 100 bar, ET= 1.5 ms; P_v=40 kPa, (a) T_f , T_n=30°C; (b) T_f , T_n=90°C and (c) T_f , T_n=120°C.

The analysis of the spray images acquired in operating conditions inducing the flash boiling phenomenon evidenced dramatic modifications of the spray structure, which are expected to result in significant modifications of the spray momentum flux distribution in space, however preserving the global momentum flux for the jet. In all the nine operating conditions analyzed in terms of imaging and global momentum flux, the momentum distributions maps over a plane orthogonal to the spray main axis where obtained at a Z=10 mm distance from the nozzle (Figure 17). In order to build the momentum flux maps, the local impact force time-history measured in each of the 127 considered positions is converted in a local pressure value and integrated in time through the entire injection process; the resulting pressure time-integral is depicted in the maps, representing the momentum flux spatial distribution when the entire injection process is considered. As can be seen, in all the examined conditions the spray momentum maps are appreciably symmetrical around the jet main axis, which is slightly deviated (about 0.5 mm) towards the positive X-coordinate. In the operating conditions in which the flash boiling phenomenon is not present (*i.e.* Pv= 303 kPa, Pv= 101 kPa − T= 30 °C and 90 °C, Pv= 40 kPa − T= 30 °C) the momentum maps is confined is an approximately ellipsoidal region with main axes length 2 mm and 3 mm, which implies the presence of a very narrow spray portion characterized by a non negligible momentum flux. When the flash boiling phenomenon is triggered, the spray momentum map is consistently enlarged (Figure 17, P_v= 40 kPa − T_f , T_n = 120°C) and it is constituted by very low momentum flux local values, so to preserve the global momentum value as observed in the global analysis. In Figure 18 the three different temperature levels (30°C (a), 90°C (b), 120°C (c)) at 40kPa of vessel pressure are reported as 3D maps of local momentum. As can be seen, the non flash-boiling condition (a) is characterized by a higher peak and by a consistently narrower base in good agreement with the imaging results. Conversely, in full flash boiling conditions (c) the momentum flux map appears to be large and smooth, with peak values less than the half of standard flow conditions. Intermediate characteristics were observed for the operating conditions pertaining the transition between flash-boiling and and no flash-boiling (b).

Conclusions

In the present paper a single-hole, research GDI injector was used to investigate the effect of the flash-boiling phenomenon on the spray evolution in terms of jet shape and momentum flux. As a preliminary characterization of the research GDI injector hydraulic operation, the mean injected volumes and the injection rate obtained at P_{rail}= 50 bar, 100 bar and 150 bar were determined to assist the momentum flux analysis in standard flow and flash-boiling conditions. Further, the spray evolution in terms of global shape, tip penetration and cone angle was investigated by means of high speed imaging. The momentum flux was examined in global and local terms, *i.e.* analyzing the momentum distribution over a surface orthogonal to the jet main axis. Both the imaging and momentum analyses were carried out with injection pressure ranging from 50 bar to 150 bar, while the vessel absolute pressure in which the spray evolved was varied between 40 kPa and 303 kPa, with the injector nozzle fixture and the fuel temperature varied from 30 °C to 120 °C. The following main conclusions can be drawn:

- The hydraulic analysis evidenced the actual influence of the rail pressure on the injection process start, obtaining a satisfactory agreement with imaging results. Further, the joint analysis of the injection rate and global momentum flux time-history allowed evidencing that these quantities are strictly correlated and can give a significant insight in the injector operation even for the unsteady phases of the injection process.
- The imaging analysis evidenced how the spray structure is completely altered in flash boiling conditions with respect to the standard (low temperature) spray evolution. The spray appears much less compact, with a large recirculating toroidal vortex around the jet tip.

- In full flash-boiling conditions (Air to Saturation Pressure Ratio below 0.3) the spray penetration is significantly reduced: at 40 kPa absolute test vessel pressure, 120 °C nozzle and fuel temperature the final tip penetration value is 40 % lower than in equal vessel pressure, 30 °C nozzle and fuel temperature condition. Correspondingly, the spray cone angle is drastically increased, rising from 4 deg to about 17 deg.
- In the transition from non-flash boiling to fully flash boiling conditions (Air to Saturation Pressure Ratio between 0.3 and 1) the spray structure appears to be significantly altered, with a reduced tip penetration and increased global cone angle.
- The flash-boiling onset does not seem to affect the global momentum flux measured by the impact method.
- In high temperature conditions, the used injector evidenced a reduced injection duration that is likely due to change operation of the electromechanical components rather than to fluid dynamic effects.
- The analysis of the local momentum flux distribution over a surface orthogonal to the spray main axis evidenced a significant enlargement of the jet fingerprint in flash boiling conditions, along with a significant decrease of the local momentum peak intensity.

Symbols and Acronyms

AtSPR - Air to Saturation Pressure Ratio, n.d.

CoV - Coefficient of Variation, %

D - Target diameter, mm

d - Injector hole diameter, mm

EMI - Einspritz Mengeindikator (Injection quantity indicator)

ET - Energizing Time, ms

EVI - Einspritz Verlaufindikator (Injection curve indicator)

f - fuel

GDI - Gasoline Direct Injection

IR - Injection Rate, mm^3/ms

L - Injector hole channel length, mm

n - nozzle

Pinj - Injection Pressure, bar

t - Time, s

V - Volume, cm3

v - Test vessel

β - Fluid Bulk Modulus, Pa

References

1. Heywood, J. B., “Internal Combustion Engine Fundamentals”, McGraw-Hill Book Co., New York, 1988.
2. Baumgarten, C.:”Mixture Formation in Internal Combustion Engines”, Springer-Verlach, 2006. ISBN-13 978-3-540-30835-5.
3. Shahed, S. and Bauer, K., “Parametric Studies of the Impact of Turbocharging on Gasoline Engine Downsizing,” *SAE Int. J. Engines* 2(1):1347-1358, 2009, doi:10.4271/2009-01-1472.
4. Xu, M., Zhang, Y., Zeng, W., Zhang, G. et al., “Flash Boiling: Easy and Better Way to Generate Ideal Sprays than the High Injection Pressure,” *SAE Int. J. Fuels Lubr.* 6(1):137-148, 2013, doi:10.4271/2013-01-1614.
5. Shengqiwu, Xu M., Zhang Y., Z G. e Li L., Analysis of Flash-boiling Spray Mechanism using a Two-Dimensional Transparent Nozzle, ILASS Americas, 2013.
6. Aleif P. e van Romunde Z., An analysis of spray development with iso-octane, n-pentane, gasoline, ethanol and n-butanol from a multi-hole injector under hot fuel conditions, Elsevier, 2013.
7. Sher E., Bar-Ko T. e Rashkovan A., «Flash-boiling Atomizations,» *Progress in Energy and Combustion Science*, n. 34, 2007.
8. S.-P. J., Romunde Z. v., Aleiferis P., R. D., W. S., e C.R.F., «Cavitation, primary break-up and flash boiling of gasoline, iso-octane and n-pentane with a real-size optical direct-injection nozzle,» *Fuel*, vol. 89, n. 2592-2607, 2010.
9. Postrioti, L., Mariani, F., Battistoni, M., and Mariani, A., “Experimental and Numerical Evaluation of Diesel Spray Momentum Flux,” *SAE Int. J. Engines* 2(2):287-299, 2010, doi:10.4271/2009-01-2772.
10. Postrioti, L. and Battistoni, M., “Evaluation of Diesel Spray Momentum Flux in Transient Flow Conditions,” SAE Technical Paper 2010-01-2244, 2010, doi:10.4271/2010-01-2244.
11. Postrioti, L., Battistoni, M., Ungaro, C., and Mariani, A., “Analysis of Diesel Spray Momentum Flux Spatial Distribution,” *SAE Int. J. Engines* 4(1):720-736, 2011, doi:10.4271/2011-01-0682.
12. Payri R., García J.M., Salvador F.J., Gimeno J., Using Spray Momentum Flux Measurements to Understand the Influence of Diesel Nozzle Geometry on Spray Characteristics, Fuel; vol. 84 (5), pp. 551-561, 2005.
13. Desantes, J., Payri, R., Salvador, F., and Gimeno, J., “Measurements of Spray Momentum for the Study of Cavitation in Diesel Injection Nozzles,” SAE Technical Paper 2003-01-0703, 2003, doi:10.4271/2003-01-0703.
14. Desantes, J., Payri, R., Salvador, F., and Gimeno, J., “Prediction of Spray Penetration by Means of Spray Momentum Flux,” SAE Technical Paper 2006-01-1387, 2006, doi:10.4271/2006-01-1387.
15. Kampmann, S., Dittus, B., Mattes, P., and Kirner, M., “The Influence of Hydro Grinding at VCO Nozzles on the Mixture Preparation in a DI Diesel Engine,” SAE Technical Paper 960867, 1996, doi:10.4271/960867.
16. Rajaratnam N., Turbulent Jets. Amsterdam, Elsevier; 1974.
17. Grimaldi C. N., Postrioti L., 2000, “Experimental Comparison between Conventional and Bio-derived Fuels Sprays from a Common Rail Injection System”, SAE Paper 2000-01-1252. SAE 2000 Transactions Journal of Engines, Section 3, Vol. 109.
18. Postrioti, L., Grimaldi, C., Ceccobello, M., and Di Gioia, R., “Diesel Common Rail Injection System Behavior with Different Fuels,” SAE Technical Paper 2004-01-0029, 2004, doi:10.4271/2004-01-0029.

19. Postrioti, L. and Ubertini, S., "An Integrated Experimental-Numerical Study of HSDI Diesel Injection System and Spray Dynamics," SAE Technical Paper 2006-01-1389, 2006, doi:10.4271/2006-01-1389.

20. Postrioti, L., Buitoni, G., Pesce, F.C., Ciaravino, C. "Zeuch method-based injection rate analysis of a common-rail system operated with advanced injection strategies", (2014) Fuel, 128, pp. 188-198.

21. Soudbakhsh, D. and Eskandarian, A., "A Collision Avoidance Steering Controller using Linear Quadratic Regulator," SAE Technical Paper 2010-01-0459, 2010, doi:10.4271/2010-01-0459.

The Engineering Meetings Board has approved this paper for publication. It has successfully completed SAE's peer review process under the supervision of the session organizer. The process requires a minimum of three (3) reviews by industry experts.

ISSN 0148-7191

http://papers.sae.org/2015-24-2480